Flash Thermal Diffusivity Measurements and Inspection of Additively Manufactured Ti-6Al-4V Specimens with Varying Process Parameters

Joseph N. Zalameda[1]*, Samuel J. A. Hocker[1], Erik L. Frankforter[1], Peter W. Spaeth[1], and Andrew R. Kitahara[2]

[1]NASA Langley Research Center Hampton, VA 23681-2199
[2]National Institute of Aerospace Hampton, VA 23666

ABSTRACT

Flash thermal diffusivity measurements were obtained on additively manufactured Ti-6Al-4V disk shaped specimens with various process parameters. For additively manufactured metal parts, processing parameters such as laser power and scanning speed are critical to ensure the desired microstructure. For this study, the laser powder bed fusion process parameters were changed at various angular sections on a 21 mm diameter and 3.0 mm thick disk. The measurement of thermal diffusivity was performed by fitting a 1-dimensional thermal model to the data pixel by pixel to produce an inspection image. The image revealed the detection of defects such as lack of fusion porosity and areas of aggregated porosity. The thermal diffusivity imagery was compared to immersion scan ultrasonic and X-ray computed tomography (CT) measurements for validation. Based on these results, additional samples were investigated using a single side thermal inspection technique to detect lack of fusion porosity and near surface voids.

Keywords: thermal nondestructive evaluation, thermal diffusivity, additive manufacturing, laser powder bed fusion, lack of fusion porosity, aggregated porosity, X-ray computed tomography, ultrasonic inspection

1. INTRODUCTION

In a framework to assist in the certification of additive manufacturing (AM) built parts, nondestructive evaluation (NDE) plays a vital role to ensure build quality. In the area of NDE, inspections can be performed during the build or after the build using various methodologies such as X-ray computed tomography (CT), ultrasound, or thermography. One area of concern is the formation of porosity for AM metal parts. Recently there has been some work to apply flash thermography to AM built parts with programmed defects representing pores or voids [1-2]. In this work we investigate using through transmission and single sided flash thermography inspections on Ti-6Al-4V AM built disk samples with varying build processing parameters.

A Configurable Architecture Additive Testbed (CAAT) is used to vary the processing parameters in a laser powder bed fusion (LPBF) AM process. A LPBF AM process involves a laser that is scanned over a bed of powder. The laser is used to melt the metal powder at precise locations layer by layer [3]. The CAAT system is comprised of an enclosed environmental chamber which has been modified to conduct LPBF experiments. The CAAT system allows for integration of various in-situ NDE sensors as well as oxygen and thermocouple sensors to document the build environment. The CAAT system allows for varying the hatch spacing, laser power and laser scanning speed. This affects the amount of energy delivered to the powder and this directly contributes to the microstructure of the AM part.

For this study, the LPBF process parameters (laser power and scanning speed) were changed at various angular sections on 21 mm diameter and 3 mm thick disks manufactured from Ti-6Al-4V powder. The disks were inspected using a through transmission flash thermography technique [4,5]. The measurement of thermal diffusivity was performed by

*joseph.n.zalameda@nasa.gov; phone 1 757-864-4793; fax 1 757-864-4914; http://nde.larc.nasa.gov

fitting a 1-dimensional thermal model to the, data pixel by pixel, to produce an inspection image. The image revealed the defects such as lack of fusion porosity and areas of aggregated porosity. The conduction of heat is impeded by the porosity. The thermal diffusivity imagery was compared to immersion scan ultrasonic and X-ray CT measurements for validation. Based on these results, additional samples were investigated using a single side thermal inspection technique to detect lack of fusion porosity and near surface voids.

2. ADDITIVE MANUFACTURING SYSTEM AND SAMPLE DESCRIPTIONS

2.1 Configurable Architecture Additive Testbed (CAAT)

The CAAT system was used to vary the process parameters to manufacture the Ti-6AL-4V disks. The CAAT system is comprised of an enclosed environmental chamber that has been modified to conduct LPBF experiments with a variety of sensors and multiple view port windows for various camera configurations. This configurable architecture system allows for the addition of sensors. Currently the chamber is fitted with a variety of sensors such as infrared cameras, visible cameras, an oxygen (< 10 ppm operation) sensor, and thermocouples. The laser was a modulated continuous emission source with wavelength of 1070 nm and a maximum power of 1 kilowatt.

2.2 Laser Powder Bed Fusion AM Samples

Four disk samples, (A, B, C, and D) shown in Figures 1, 2, and 9, were fabricated with Ti-6Al-4V powder and included a variety of processing parameters combined with specific angular zones to create a wide range of localized process conditions. The angular zones were built with varied laser powers and velocity combinations. Low laser powers with fast scanning velocities resulted in low surface energy densities yielding lack of fusion porosity [6,7]. High laser power and slow velocities result in high delivered surface energy densities that can result in keyhole porosity [7]. A balanced combination of print parameters, power, velocity, and hatch spacing, are expected to result in fully consolidated areas. Angular zone 2 in disks A, C, and D was printed with very low relative surface energy densities that resulted in a very high degree of lack of fusion porosity. Angular zones 1-3 in disk B were printed with low surface energy densities and lack of fusion porosity [8]. To allow for the thermal diffusivity measurements, disk samples A and B were polished to a uniform thickness of 2.90 +/- 0.12 mm and 3.07 +/- 0.05 mm respectively.

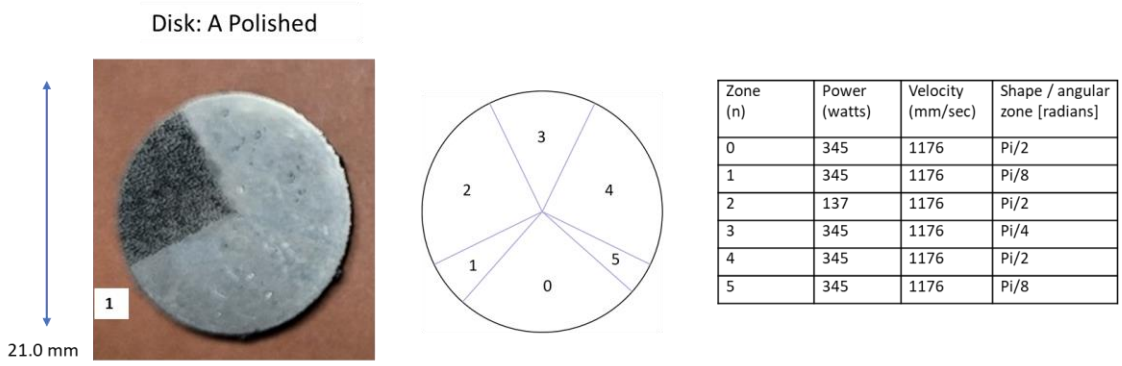

Zone (n)	Power (watts)	Velocity (mm/sec)	Shape / angular zone [radians]
0	345	1176	Pi/2
1	345	1176	Pi/8
2	137	1176	Pi/2
3	345	1176	Pi/4
4	345	1176	Pi/2
5	345	1176	Pi/8

Figure 1: Picture of polished disk sample with six processing parameter angular zones.

3. THERMAL DIFFUSIVITY MEASUREMENT SYSTEM AND RESULTS

3.1 Thermal Measurement Systems

The through transmission and single side thermal inspection systems are shown in Figures 3a and 3b respectively. For the through transmission thermal inspection system, the test specimen is placed between the heat source (flash lamp) and the infrared camera. The lamp used to induce the heat was a commercially available photographic flash lamp powered by a 1200 joule power supply. A glass filter was placed over the flash lamp opening to suppress background infrared after

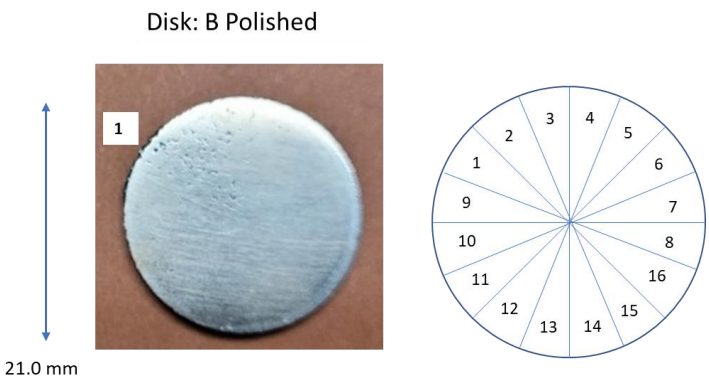

Zone (n)	Power (watts)	Velocity (mm/sed)	Shape / angular zone [radians]
1	221	1176	Pi/8
2	221	1092	Pi/8
3	221	1008	Pi/8
4	221	924	Pi/8
5	221	840	Pi/8
6	221	756	Pi/8
7	221	672	Pi/8
8	221	588	Pi/8
9	308	1175	Pi/8
10	308	1092	Pi/8
11	308	1008	Pi/8
12	308	924	Pi/8
13	308	840	Pi/8
14	308	756	Pi/8
15	308	672	Pi/8
16	308	588	Pi/8

Figure 2: Picture of polished disk sample with sixteen processing parameter equiangular zones.

firing the flash lamp. The camera used was a 640 x 512 indium antimonide (InSb) array operating in the 3 - 5 micron infrared band. A 50 mm focal length germanium lens was used. The image data frame rate was 100 image frames per second. The data acquisition software was custom developed, and the flash lamp was triggered by the data acquisition computer. The computer recorded the infrared image of the specimen immediately prior to the firing of the flash lamp (for emissivity correction by background subtraction), then the thermal response of the specimen is acquired. For the disk specimens a total of 300 frames were acquired and the data acquisition time was 3.0 seconds. The single side thermal inspection system shown in Figure 3b has the flash lamp and infrared camera configured on the same side as the samples. The commercially available system used an infrared camera with a 640 x 512 indium antimonide (InSb) array operating in the 3 - 5 micron infrared band. The system used a photographic flash lamp powered by two 4300 joule power supplies. The image data frame rate was 120 image frames per second. A 50 mm focal length germanium lens was used.

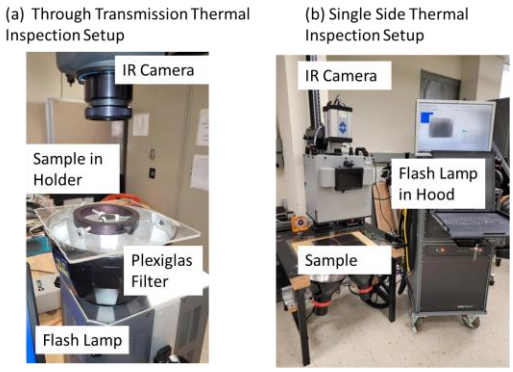

Figure 3: Picture of through transmission and single side thermal inspection systems.

3.2 Thermal Diffusivity Measurement and Results

Through transmission flash thermography is based on conduction of heat through the sample. This technique is quantitative wherein thermal diffusivity is measured [4,5]. Variation in the thermal diffusivity due to defect areas can be imaged with this technique. For example, porosity or gas filled voids can lower the thermal diffusivity as compared to solid regions. The single layer thermal model is given in Equation 1 where l is the thickness, t is time, $Tmax$ is the maximum sample temperature, and α is the thermal diffusivity. For a known thickness, the thermal response model (Equation 1) was fitted to the data, pixel by pixel, to the obtain both thermal diffusivity and $Tmax$. An example

$$T(t) = \begin{cases} 2\,T_{max}\sqrt{\frac{l^2}{\pi\,\alpha\,t}}\left(e^{-\frac{l^2}{4\,\alpha\,t}} + e^{-\frac{9l^2}{4\,\alpha\,t}}\right), t < 0.4\,\frac{l^2}{\alpha} \\ 2\,T_{max}\left(1 - e^{-\frac{\alpha\,t\,\pi^2}{l^2}}\right), t \geq 0.4\,\frac{l^2}{\alpha} \end{cases} \quad (1)$$

curve fit for a given pixel is shown in Figure 4. This processing technique is typically more effective than Parker's method [4] which uses one point in time to determine thermal diffusivity. The curve fitting was performed for a time window of 0.1 to 1.0 seconds after the flash.

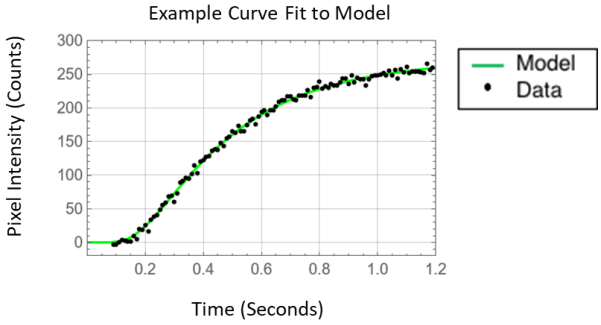

Figure 4: Example model fit to the data for a single pixel point.

The thermal diffusivity images are shown for the six and sixteen angular zones disk samples in Figures 5 and 6 respectively. The samples were painted to enhance emissivity with a flat black paint on both sides. The literature thermal diffusivity value for solid Ti-6AL-4V (Grade 5) at room temperature is 0.029 cm^2/sec [9]. The brighter area around the circumference was due to heat flow edge effects and this circular region was ignored. For each angular section, a 10 x 10 pixel square area was selected approximately 1/3 of the radius from the center to obtain a mean thermal diffusivity. These values are provided in the tables shown in Figures 5 and 6 and allows for comparison to the processing parameters.

The six angular section sample (disk A) clearly shows zone 2, which is the area corresponding to lower thermal diffusivity value = 0.0186 cm^2/sec due to the lack of fusion porosity. It is noted that within the lack of fusion area, variations can be seen within where some spots have a particularly lower thermal diffusivity. The zones 0, 1, 3, 4, and 5 appear uniform with no significant variation in diffusivity with a mean value of 0.0256 cm^2/sec. This is significantly lower than the literature value of Ti-6Al-4V and therefore indicates the presence of small pores. It is expected that individual pores would not be detectable unless they were large and near the surface. This is revealed in disk B sample. The sixteen angular section sample (disk B) is shown in Figure 6 and indicates areas of lower thermal diffusivity in zones 1, 2, and 3 (average value of 0.0255 cm^2/sec) as compared to zones 9, 10, and 11 which appear to have a slightly higher thermal diffusivity (average value of 0.0266 cm^2/sec). The laser power and scanning speed for zones 1, 2 and 3 have lower laser power and high scanning speed, and this would result in lack of fusion porosity. It is noted that there can be seen variations within zones 1, 2 and 3 where some spots (noted a, b, and c), in Figure 6, have a particularly lower thermal diffusivity of 0.0250, 0.0247, and 0.0241 cm^2/sec respectively. These areas are large voids and will be compared with X-ray CT.

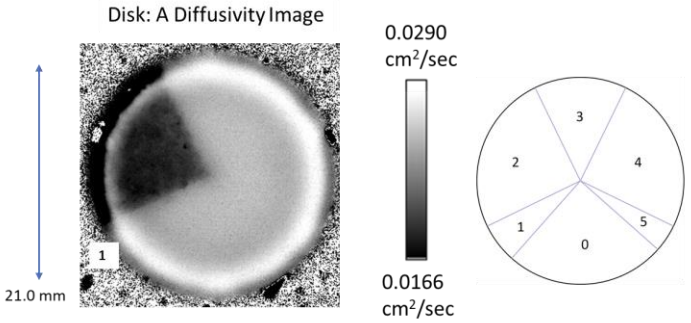

Zone (n)	Power (watts)	Velocity (mm/sec)	Shape / angular zone [radians]	Thermal Diffusivity (cm^2/sec)
0	345	1176	Pi/2	0.0258 +/-0.00043
1	345	1176	Pi/8	0.0253 +/-0.00036
2	137	1176	Pi/2	0.0186+/-0.00031
3	345	1176	Pi/4	0.0256 +/-0.00040
4	345	1176	Pi/2	0.0258 +/-0.00038
5	345	1176	Pi/8	0.0257 +/-0.00050

Figure 5: Thermal diffusivity imaging results for the 6 angular section disk A sample.

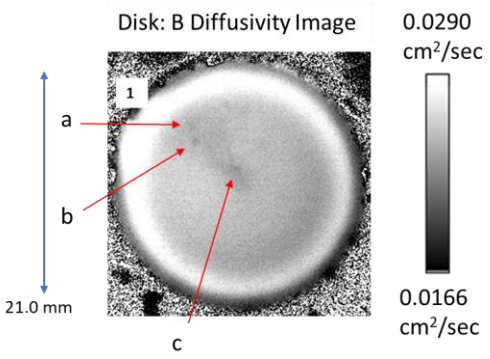

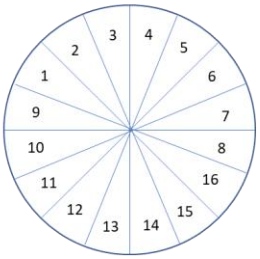

Zone (n)	Power (watts)	Velocity (mm/sec)	Shape / angular zone [radians]	Thermal Diffusivity (cm^2/sec)
1	221	1176	Pi/8	0.0256 +/-0.00052
2	221	1092	Pi/8	0.0253 +/-0.00055
3	221	1008	Pi/8	0.0257 +/-0.00055
4	221	924	Pi/8	0.0258 +/-0.00061
5	221	840	Pi/8	0.0258 +/-0.00054
6	221	756	Pi/8	0.0257 +/-0.00048
7	221	672	Pi/8	0.0256 +/-0.00046
8	221	588	Pi/8	0.0253 +/-0.00055
9	308	1175	Pi/8	0.0267 +/-0.00052
10	308	1092	Pi/8	0.0267 +/-0.00052
11	308	1008	Pi/8	0.0264 +/-0.00052
12	308	924	Pi/8	0.0261 +/-0.00054
13	308	840	Pi/8	0.0257 +/- 0.00054
14	308	756	Pi/8	0.0257 +/-0.00051
15	308	672	Pi/8	0.0254 +/-0.00053
16	308	588	Pi/8	0.0252 +/-0.00052

Figure 6: Thermal diffusivity imaging results for the sixteen equiangular section disk B sample.

3.3 Comparison to X-ray CT

X-ray CT measurements, on disk B, were analyzed to investigate the small areas a, b, and c of low thermal diffusivity shown in Figure 6. The voxel resolution of the X-ray CT was approximately 0.0127 mm for a given X, Y, Z direction. A transverse X-ray CT slice is shown in the middle image of Figure 7 along with the diffusivity image of disk B (left image), and a vertical slice X-ray CT image (right image). The X-ray CT image for defect b corresponded to a depth of approximately 0.23 mm from the top surface and revealed defect b to be a large void. Based on these results, other samples were investigated using a single side thermal inspection to detect near surface voids.

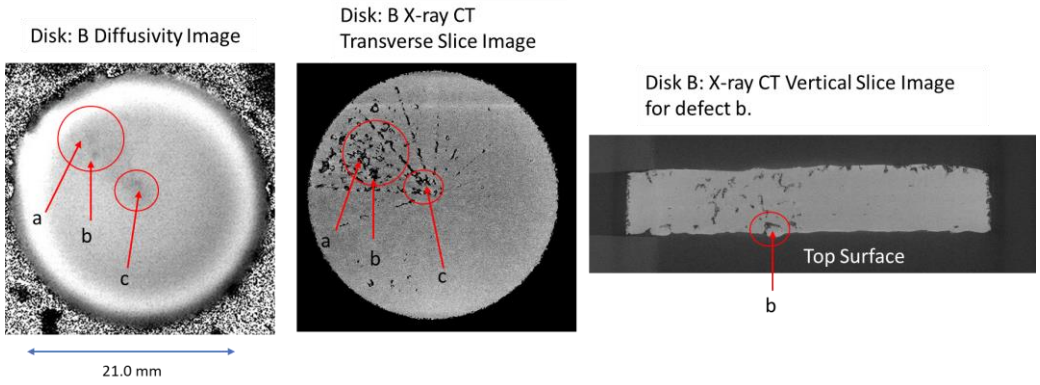

Figure 7: Comparison of disk B X-ray CT to thermal diffusivity image.

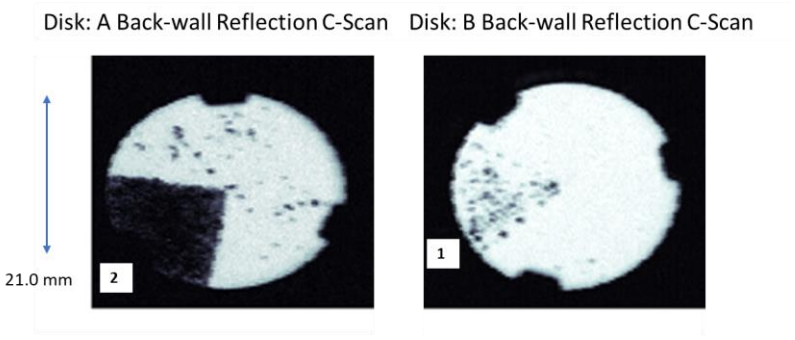

Figure 8: Ultrasonic C-scan images of the back-wall reflection for disks A and B.

3.4 Comparison to Ultrasonic Inspections

The disk samples A and B were inspected in an ultrasonic (UT) immersion scan pulse-echo mode as shown in Figure 8. The disks were placed into an optical lens mount. A 25 MHz focused transducer was used, and the specimens were placed at the as-manufactured focal length by setting the transducer height to the location that maximized the reflection off the specimen's top surface. Raster scans were performed in 0.13 mm horizontal and vertical increments, and resulting waveforms digitized at 16 bits with a sample rate of 180 MS/s. Shown in Figure 8 are the back-wall reflection ultrasonic C-scan images of disks A and B where the dark areas reveal, qualitatively, loss of reflected energy due to lack of fusion porosity (section 2 of disk A) and large voids (small dark areas shown for both disks A and B). It is noted that for disk A, porosity areas were scattered across the sample; however, the thermal diffusivity imaging did not capture these areas. This could be due to the depth of the voids where the heat flow contrast is lost at the surface. There is a region of disk B, left-hand side angular zones 1-3 in Figure 8 showing porosity indications, which agrees with the X-Ray CT and the thermal diffusivity results in Figure 7.

4. SINGLE SIDED THERMAL CONFIGURATION FOR IN-SITU INSPECTIONS DURING AM BUILDS

4.1 Single Side Inspection Measurement and Samples

The single side thermal inspection system used is shown in Figure 3b. This is a more practical inspection setup since only one side of the sample is required so a measurement system could be implemented in an AM build chamber and the inspection can be performed in-situ as the layers are built. During a build, the surface thickness is typically not uniform as shown in Figure 9 of two unpainted and unpolished disks: C and D, and therefore an exact measurement of thermal diffusivity can be difficult. However, changes in how the surface cools down after heating can reveal near surface defects if the surface is not reflective (surface emissivity is not too low). Significant reflection from the heat lamps, after the flash, can potentially induce a time dependent signal that can mask the inspection. For these two disk samples, the build parameters are nearly equivalent to disk A discussed previously. Similarly, the angular section zone 2 build parameters with a laser power of 137 watts and a laser scanning speed of 1176 mm/sec, result in a low thermal diffusivity area due to lack of fusion porosity.

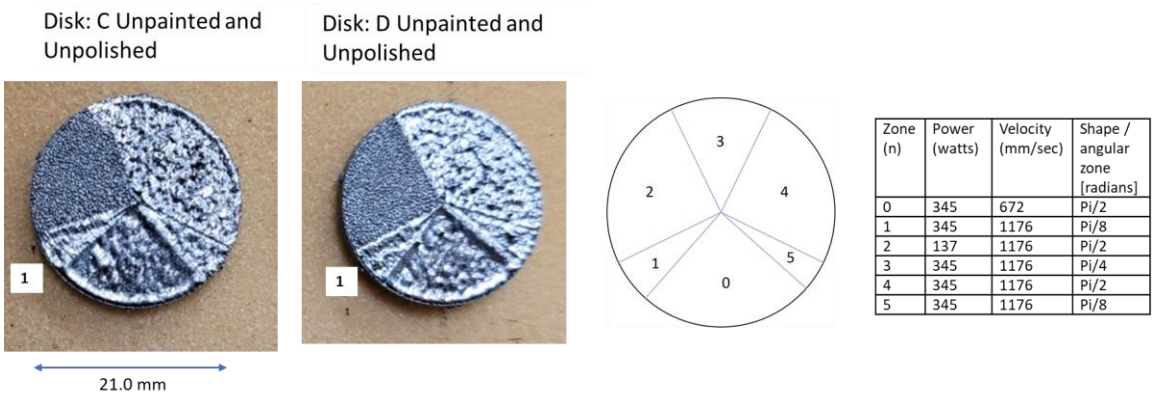

Zone (n)	Power (watts)	Velocity (mm/sec)	Shape / angular zone [radians]
0	345	672	Pi/2
1	345	1176	Pi/8
2	137	1176	Pi/2
3	345	1176	Pi/4
4	345	1176	Pi/2
5	345	1176	Pi/8

Figure 9: Unpolished and unpainted disks C and D, both with the same processing parameters per angular zone.

4.2 Single Side Inspection Results

Principal component analysis (PCA) was used to analyze the single side thermal inspections for disks C and D. PCA is a common processing technique for thermal data [10]. This algorithm is based on decomposition of the thermal data into its principal components or eigenvectors. Flash thermography signals are slowly decaying waveforms and therefore the predominant variations are usually contained in the first or second eigenvectors. This accounts for the data variance of interest. The principal components are computed by defining a data matrix A where the time variations are along the

columns and the spatial image pixel points are row-wise. The matrix A is adjusted by dividing the maximum value (normalization) and subtracting the mean along the time dimension. The covariance matrix is defined as A^TA. The covariance matrix is now a square matrix of order equal to the number of images used for processing. The covariance

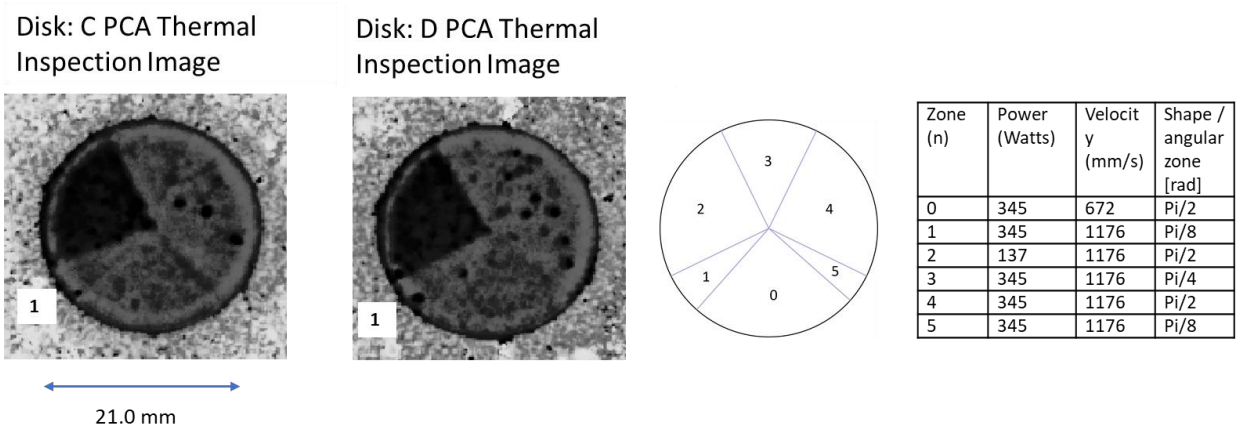

Zone (n)	Power (Watts)	Velocity (mm/s)	Shape / angular zone [rad]
0	345	672	Pi/2
1	345	1176	Pi/8
2	137	1176	Pi/2
3	345	1176	Pi/4
4	345	1176	Pi/2
5	345	1176	Pi/8

Figure 10: PCA thermal inspection results on unpolished and unpainted disks C and D.

matrix can then be decomposed into its eigenvalues and eigenvectors. The PCA inspection image is calculated by dot product multiplication of the selected eigenvector times the temperature response (data matrix A), pixel by pixel. The inspection results are shown in Figure 10. The thermal inspection results were calculated using the 2nd eigenvector. The flash heating was on the 10th image and the images processed were from the 20th to 80th image representing a time window of 0.083 – 0.583 seconds and therefore the inspection time requires less than 1 second. The dark areas represent areas proportional to low thermal diffusivity resulting from near surface lack of fusion porosity or large voids. Shown in Figure 11 is a comparison of disk D thermal inspection to X-ray CT for some of the larger indications. The larger indications are circled in the X-ray CT image and reveal near surface voids. These voids affect the diffusion of heat as indicated by the thermal inspection image.

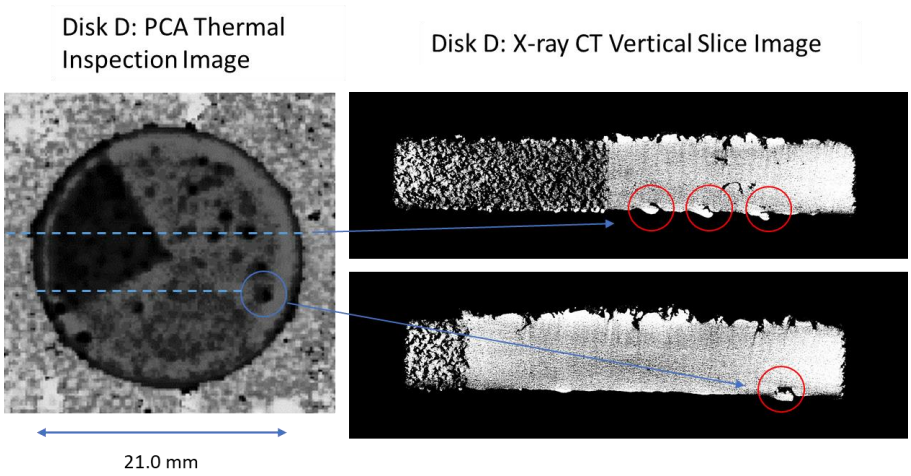

Figure 11: Example comparisons of PCA thermal inspection results to X-ray CT for disk D.

5. CONCLUSIONS

The measurement of thermal diffusivity was performed by fitting a 1-dimensional thermal model to the data pixel by pixel to produce an inspection image. The diffusivity imaging results revealed the detection of defects such as lack of fusion porosity and areas of large porosity. Small differences in the build parameters did not reveal significant changes in the measured thermal diffusivity, however, compared to the literature value of Ti-6Al-4V the thermal diffusivity values measured overall were consistently lower, thus indicating the influence of porosity. This was especially true for the large pore areas shown in Figure 6 and compared to the X-ray CT in Figure 7. The ultrasonic C-scan of disk B, left-hand side angular zones 1-3 in Figure 8 revealed areas of porosity indications which agreed with the X-Ray CT and the thermal diffusivity results of Figure 7.

The single side thermal inspection technique clearly revealed the ability to detect changes in thermal diffusivity due to near surface pores and areas of lack of fusion porosity. The inspection was performed on unpolished and unpainted samples. This technique is advantageous for as-manufactured AM parts with rough surfaces, compared to ultrasonic measurements which typically require a smooth surface. The single side thermal inspection technique is more practical since access to one side of the sample is required, therefore a measurement system could be implemented into an AM build chamber. Additionally, the inspection can be performed in-situ as the layers are built.

Data fusion between process monitoring and the inspection techniques studied (ultrasound, X-ray CT, and thermal) could be used for complementary quantitative flaw detection with registration to the process parameters. Future work could include compiling all data sources into a centralized data repository and to develop schema to support sensor-to-sensor and part-to-part build documentation/assessment.

ACKNOWLEDGEMENTS

The authors would like to thank William P. Sommers of the Nondestructive Evaluation Sciences Branch for the X-ray CT measurements. Also, the authors would like to thank the Transformational Tools and Technologies Project of the NASA Transformative Aeronautics Concepts Program for support of this work.

REFERENCES

[1] Accardi, Ester D' et al 2021 IOP Conf. Ser.: Mater. Sci. Eng. 1038 012018.
[2] Wallace, N. J., Crane, N. B., and Jones, M. R., "Defect Measurement Limits using Flash Thermography with Application to Additive Manufacturing", NDT & E International, Volume 128, June 2022, 102615.
[3] Yap, C.Y., Chua, C.K., Dong, Z.L., Liu, Z.H., Zhang, D.Q., Loh, L.E., and Sing, S.L., Review of Selective laser melting: Materials and applications, Applied Physics Reviews 2, 041101 (2015); doi:10.1063/1.4935926.
[4] Parker W. J., Jenkins R. J., Butler C. P., and Abbott G. L., "Flash Method of Determining Thermal Diffusivity, Heat Capacity, and Thermal Conductivity," Journal of Applied Physics, Vol. 32 #9, pp. 1679 – 1684, September 1961.
[5] W. P. Winfree and D. M. Heath, "Thermal diffusivity imaging of aerospace materials and structures," Proceedings of SPIE, Thermosense, XXIII 3361, pp. 282–290 (1998).
[6] Tang, M., Pistorius, P.C., Beuth, J.L., 2017. Prediction of lack-of-fusion porosity for powder bed fusion. Additive Manufacturing 14, 39–48. https://doi.org/10.1016/j.addma.2016.12.001.
[7] Cunningham, R., Narra, S.P., Montgomery, C. et al. Synchrotron-Based X-ray Microtomography Characterization of the Effect of Processing Variables on Porosity Formation in Laser Power-Bed Additive Manufacturing of Ti-6Al-4V. JOM 69, 479–484 (2017). https://doi.org/10.1007/s11837-016-2234-1.
[8] Hocker, S.J.A., Richter, B., Spaeth, P.W., Kitahara, A.R., Zalameda, J.N., Glaessgen, E.H., 2023. A Point Field Driven Approach to Process Metrics Based on Laser Powder Bed Fusion Additive Manufacturing Models and In-Situ Process Monitoring. JMR. https://doi.org/10.1557/s43578-023-00953-7.
[9] ASM Aerospace Specification Metals Inc., Titanium Ti-6Al-4V (Grade 5), Annealed, ASM Material Data Sheet (matweb.com), Accessed March 29, 2023.
[10] Rajic, N., "Principal Component Thermography for Flaw Contrast Enhancement and Flaw Depth Characterisation in Composite Structures", Composite Structures, Vol. 58, pp. 521--528, (2002).